ELSEVIER

Computer Physics Communications 118 (1999) 11–16

Computer Physics Communications

www.elsevier.nl/locate/cpc

A combined molecular dynamics and finite element method technique applied to laser induced pressure wave propagation

Julia A. Smirnova, Leonid V. Zhigilei, Barbara J. Garrison

Department of Chemistry, 152 Davey Laboratory, The Pennsylvania State University, University Park, PA 16802, USA

Received 21 August 1998

Abstract

Analysis of a variety of dynamic phenomena requires simultaneous resolution at both atomistic and continuum length scales. A combined molecular dynamics and finite element method approach, which we discuss in this paper, allows us to find the balance between the necessary level of detail and computational cost. The combined method is applied to the propagation of a laser-induced pressure wave in a solid. We find good agreement of the wave profile in the molecular dynamics and finite element regions. This computational approach can be useful in cases where a detailed atomic-level analysis is necessary in localized spatially separated regions whereas continuum mechanics and thermodynamics is sufficient in the remainder of the system.

PACS: 02.70.Ns; 02.70.Dh; 61.80.Az

Keywords: Multiscale simulation; Molecular dynamics; Finite-element method; Laser ablation

1. Introduction

Over the years a number of approaches have been developed to simulate dynamics in condensed phases. In the atomistic regime, the molecular dynamics (MD) simulation technique has been successfully applied to a variety of phenomena including structures of liquids [1], energetic particle bombardment of solids [2], reactions at surfaces [3], and crack propagation [4,5]. On the other hand, the finite element (FE) method is successful in modeling propagation of elastic waves and heat transfer through material at macroscopic length scales [6,7]. A schism arises, however, when one wants to examine phenomena that occur at an intermediate length regime and yet still retain an atomic-level resolution in some regions of interest. In principle, one could make MD simulations larger but even simulations with $\sim 10^6$–10^8 particles are not sufficiently large to deal efficiently with situations such as propagation of the pressure waves developed in simulations of laser ablation [8], energetic cluster impact [9] or crack propagation [4,5,10].

In particular, the generation of strong pressure waves is a natural result of the fast energy deposition in short pulse laser ablation [8,11,12]. The development and propagation of these waves occur at length scales that are beyond the capability of the MD simulation technique [8,11]. One problem is that a pressure wave reflected from the boundaries of the MD computational cell can interfere with the processes in the ablation region and hinder interpretation of the results of the simulation. Recently we developed a simple and computationally efficient approach for simulating the non-reflecting propagation of a pres-

0010-4655/99/$ - see front matter
PII S0010-4655(98)00175-1

sure wave out from the MD computational cell [11]. While providing an efficient way to avoid artifacts due to pressure wave reflection, the non-reflecting boundary conditions are not sufficient for more challenging scenarios in which there are several regions where molecular-level analysis is needed. For example, in addition to ablation at the front side of the irradiated sample, the interaction of the laser induced compressive pressure pulse with the back surface of the target can cause the desorption of the molecules adsorbed at the back surface, an effect known as acoustic desorption [13], or lead to the failure process known as back spallation [12]. Moreover, in many heterogeneous systems such as pigmented biological tissues [11,14] or polymer films containing graphitic nanoparticle sensitizers [15], the ablation or damage mechanisms are defined by intensive processes occurring in the immediate vicinity of the spatially localized absorbers embedded in a transparent medium. While the sizes of the systems of interest in these cases are far beyond the capabilities of the MD method, the areas where an atomic or molecular level analysis is necessary can be small enough to be amenable to a treatment by the MD method. The rest of the system, where relative displacements of the atoms are small, can be treated by the use of continuum mechanics and thermodynamics.

A natural approach to the simulation of multiscale processes, thus, is to combine a MD simulation for the critical regions within the system with a FE method for a continuum description of the remainder of the system. There have been a number of works where the FE method is used to simulate an adequate static [10,16,17], and dynamic [10] response of surrounding material to the processes in the MD computational cell. In the present work we demonstrate that application of a combined MD–FE technique can be extended to a multiscale simulation of a system with multiple interacting MD and FE regions.

Here we test this approach on the propagation of a laser induced pressure wave from the ablation region through a micrometer-sized sample using a two-dimensional (2D) model. The extension to three dimensions is straightforward and is currently under development. The computational method is described in Section 2, and the application of the method to the propagation of a pressure wave through the successively arranged MD, FE, and another MD region of the model is given in Section 3.

2. Computational method

A computational approach for multiscale dynamic simulations that combines molecular and continuum descriptions of different parts of the system is outlined in this section. We give the essence of the MD and FE techniques, show the computational similarities, and discuss a simple prescription for combining the two methods.

In MD simulations a computational cell is represented by a set of N particles with coordinates $\{\boldsymbol{r}_i\}$ and momenta $\{\boldsymbol{p}_i\}$. The time evolution of the system is governed by Newton's second law,

$$m_i\, d^2\boldsymbol{r}_i/dt^2 = -\nabla_i U(\boldsymbol{r}_1, \boldsymbol{r}_2, \ldots, \boldsymbol{r}_N)\,, \tag{1}$$

where m_i is the mass of the ith particle, $\boldsymbol{F}_i = -\nabla_i U(\boldsymbol{r}_1, \boldsymbol{r}_2, \ldots, \boldsymbol{r}_N)$ is the force acting on the ith particle due to interaction with other particles in the system, and $U(\boldsymbol{r}_1, \boldsymbol{r}_2, \ldots, \boldsymbol{r}_N)$ is the interaction potential. The initial positions and velocities of the particles together with the interaction potential define the whole set of thermodynamic, elastic and mechanical properties of the model material.

The set of $3N$ second-order differential equations, Eq. (1), is often solved by recasting it as a set of $6N$ first-order Hamilton's equations of motion,

$$\begin{aligned} d\boldsymbol{p}_i/dt &= -\nabla_i U(\boldsymbol{r}_1, \boldsymbol{r}_2, \ldots, \boldsymbol{r}_N)\,, \\ d\boldsymbol{r}_i/dt &= \boldsymbol{p}_i/m_i\,. \end{aligned} \tag{2}$$

Given the initial positions and momenta of the system, integration of Eq. (2) yields the total trajectory of the system. With a knowledge of the trajectories of all the particles, one can calculate spatial and temporal distributions of energy, temperature and pressure, as well as monitor the structural and phase changes in the system.

In the FE method the continuum system is divided into a finite number of elements which are usually much larger than an individual particle in a MD simulation. Each element is characterized by its geometry, a sequence of points or nodes on its periphery, and by a set of properties of the material. In particular, triangular plane-stress elements, used in 2D simulations discussed in the next section, are shown in Fig. 1. The

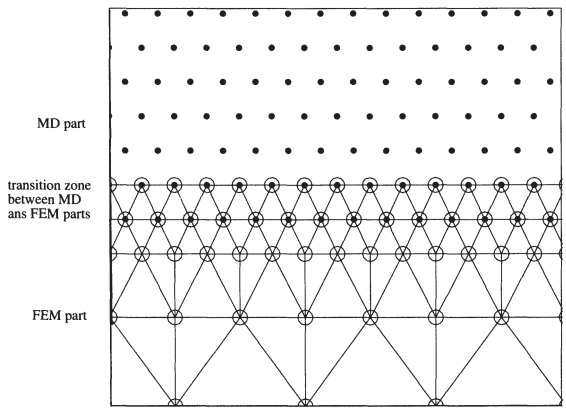

Fig. 1. Transition zone between the MD and FE regions of the system. Black dots represent MD particles. Open circles represent FE nodes. Open circles with black dots inside represent node-particles in the transition layer.

dynamics of a non-dissipative medium is defined, in the linear approximation, by the following equation for the displacements, $\boldsymbol{a}$, of a set of n nodes,

$$\mathbf{M}\, d^2\boldsymbol{a}/dt^2 = -\mathbf{K}\boldsymbol{a} + \boldsymbol{F}_{\mathrm{ex}}\,. \tag{3}$$

In this system of n coupled second-order differential equations, $d^2\boldsymbol{a}/dt^2$, is a vector of nodal accelerations, **M** is a mass matrix defined by the geometry of the elements and the density of material, **K** is the stiffness matrix that is defined by the geometry of the elements and elastic moduli of material, and $\boldsymbol{F}_{\mathrm{ex}}$ is the external force applied to the nodes. The techniques for construction of a FE mesh and calculation of mass and stiffness matrices appropriate for the simulation of a particular system are covered in an extensive literature, see for example Ref. [18].

A dynamic simulation with both MD and FE techniques involves integration of the equations of motion, Eqs. (1) and (3). An apparent similarity of Eqs. (1) and (3) suggests the possibility for coupling of the two dynamic simulation techniques. From one perspective, if the interaction potential used in the MD method is assumed to be harmonic, then $\nabla_i U$ becomes a linear function of displacement as in Eq. (3). From the other side, the stiffness matrix, **K**, is defined by the elastic constants of the system [18] and calculation of the elastic constants from a given functional form of the interaction potential is straightforward [10]. Thermal effects, damping, and nonlinearity can be introduced into the finite-element analysis [6,7,10,18] providing a more accurate match with the properties of MD system defined by a realistic interaction potential.

In order to effectively combine the regions described by the MD and FE methods into a single model, one not only has to ensure consistency between the properties of the discrete and continuum media, but also to provide a smooth transition between the two media. In the present work the coupling of the two descriptions of the media is brought about by a transition zone in which the FE nodes coincide with the positions of the particles in the MD region, Fig. 1. The width of the transition zone is equal to the cutoff distance of the interaction potential used in the MD region, two layers of particles in this case. This provides a complete set of neighbors within the interaction range for all particles in the MD region. Particles that belong to the transition zone interact via the interaction potential with the MD region. At the same time the transition zone constitutes a part of the FE grid, where the nodes coincide with the MD particles, and experience the nodal forces due to the FE grid. The forces exerted on the particle-nodes in the transition zone due to the interaction with the MD region make up the external forces $\boldsymbol{F}_{\mathrm{ex}}$ in the equations of motion for the FE nodes, Eq. (3). $\boldsymbol{F}_{\mathrm{ex}}$ is nonzero only in the transition zone between the MD and continuum regions. In order to avoid a density mismatch at the boundary, the mass at each node in the transition zone is set equal to the mass of the MD particle. Both Eqs. (1) and (3) are solved using the same integration scheme, which increases the stability in the transition region.

3. Application to laser ablation

In this section we illustrate the computational efficiency and accuracy of the combined MD and FE approach. The method is applied to the multiscale simulation of laser ablation of a molecular solid and propagation of a laser induced pressure wave from the ablation region through a micrometer-sized sample. The schematic view of the model consisting of the successively arranged MD, FE, and another MD region is shown in Fig. 2.

A relatively small surface region, part A in Fig. 2, where complex processes of laser energy deposition, overheating, buildup of high pressure, disintegration

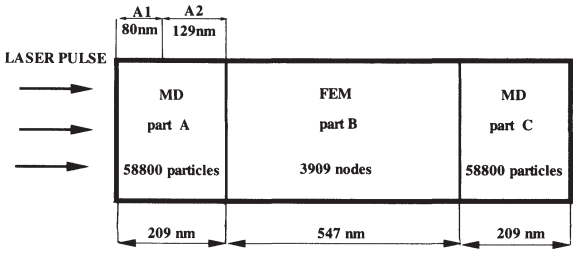

Fig. 2. Schematic picture of the model system.

and ejection of a significant amount of material are occurring, does require a molecular level analysis and is simulated by the MD method. A breathing sphere model for MD simulations of laser ablation [8] has significantly expanded the time and length scales accessible for this molecular level simulation and has provided insight into the microscopic mechanisms of laser ablation and damage of organic solids [8,11,19,20]. In this work we use a 2D version of the breathing sphere model, described in detail in Ref. [8], for simulation of the surface region of the irradiated sample.

The high pressure associated with the fast energy deposition and ablative recoil lead to the development of a pressure wave that propagates deeper into the sample [8]. The long-range propagation of the pressure wave is simulated using the FE method, part B in Fig. 2. In this work the FE part of the system is described within the linear approximation with triangular elements [18] under plane stress conditions [21]. Generally, complete compatibility between the MD and FE regions requires implementation of nonlinear elasticity and inclusion of anisotropy of the material in the FE method [10]. Introduction of nonlinearity into the FE method involves an adjustment of the stiffness matrix at each integration step whereas anisotropy increases significantly the number of nonzero elements in the stiffness matrix [6,7,22]. Although neither of these factors make an apparent problem, the stiffness matrix in this simple test case could, in principle, be ~ 60 million double precision numbers. We have thus made efforts to use only the nonzero elements to save computer memory. Thus for this first test case, we chose to use an isotropic and linear stiffness matrix. In order to partially account for nonlinearity within our linear isotropic FE continuum, we calculate the stiffness matrix based on an effective elastic modulus obtained from the average velocity of the pressure wave propagation in the MD region. This approximation allows us to decrease energy reflection at the boundary between the MD and FE parts as compared to the simulation with an elastic modulus obtained from the interaction potential [10,21]. The value of the effective 2D Young's modulus used in the stiffness matrix is 0.27 eV/Å^2, 22% higher than the one obtained from the interaction potential. A value of $1/3$ is used for Poisson's ratio of a two-dimensional isotropic material [21]. A regular triangular mesh with 145 rows of elements along the direction of the pressure wave propagation is used to represent the continuum region. The internode distance varies from 0.58 nm in the transition layer, which corresponds to the interparticle distance in the MD region (Fig. 1), to 4 nm in the bulk. Of the total number of 3909 finite-element nodes about one third are in the vicinity of the MD regions in order to provide a smooth transition from the small elements in the transition region to the larger elements in the middle of the continuum region.

The third part of the system, marked as part C in Fig. 2, is a region at the back of the sample. The interaction of the laser induced pressure wave with the back surface can cause a mechanical damage in the surface region [12] or lead to the desorption of the adsorbed molecules [13]. In order to study the microscopic mechanisms of the damage and desorption in part C, we have to switch back from the continuum FE method in part B to a molecular level MD method.

Thus, the complete computational cell (Fig. 2) contains 117600 MD particles in two MD regions, a finite-element mesh with 3909 nodes, and 560 particle-nodes in two transition zones. The size of the system is 81 by 965 nm. Periodic boundary conditions in the direction parallel to the surface are imposed, thus the effects of the edges of the laser beam are neglected and a plane pressure wave propagates from the ablation region. The laser penetration depth is 32 nm and the laser pulse duration is 15 ps. The MD regions consume most ($\sim 98\%$) of the computer time in the simulation.

The computational setup described above is used to simulate the propagation of a compressive pressure wave within the irradiated sample. Fig. 3 shows the pressure profile at different times following irradiation with a 15 ps laser pulse. The pressure wave generated in the ablation region reaches the first transition zone approximately 60 ps after the start of the laser pulse. From 60 ps to 245 ps the wave moves through the FE

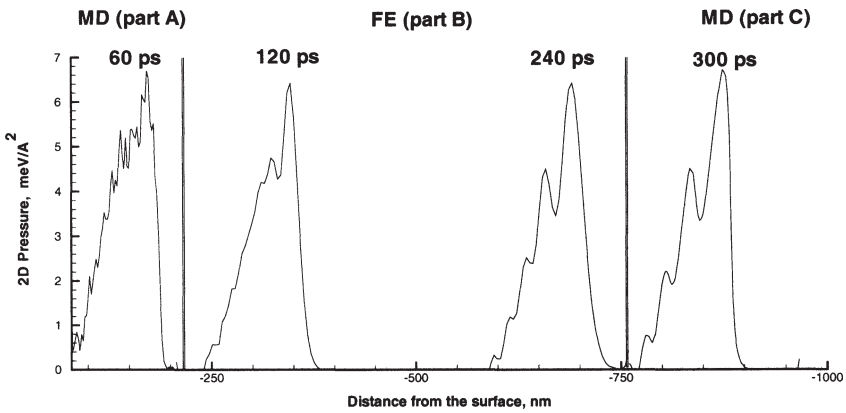

Fig. 3. The propagation of the pressure wave through the different regions of the model sample. Pressure profiles are shown for four different times after the start of the 15 ps laser pulse.

region and by 245 ps it reaches the second MD region. We observe a good agreement in the wave profile shape in all three regions of the model (parts A, B, and C). There are, however, a few changes in the wave profile. First, the wave front becomes less steep after passing through the first transition region. Second, there is an apparent smoothing of the wave profile as it has propagated to the FE region. Both of these differences are ramifications of having a molecular resolution in the MD region and a more course grid in the FE region. The high spatial resolution of the pressure wave simply cannot be described by the FE grid. Third, while the pressure wave propagates through the FE region, additional peaks spaced by 10–20 nm appear on the wave profile. The spacings between the peaks correspond to the characteristic frequencies of the FE grid. It appears that the sharp front of the pressure wave has caused a ringing in the FE grid. It is, of course, desirable to eliminate these differences. To accomplish this, however, would demand that the FE method resolution be the same as in the MD region. The wave propagates through the second transition zone between the FE and MD regions (parts B and C) without changes because in this case the wave is going from a course grid to a finer MD resolution.

In order to test additionally the combined MD–FE approach, we performed a large-scale MD simulation with a 310 nm long computational cell consisting of 86800 particles. Propagation of the laser induced pressure wave from the ablation region to the back side of this computational cell takes about 100 ps. The pressure distributions at 100 ps in the combined MD–FE model and in the pure MD model are shown in Fig. 4. Except for differences due to the smoothing in going from the fine MD resolution to the course FE grid, both profiles have the same amplitude and shape. Comparisons of the energy in these two models indicate that only $\sim 5\%$ of the pressure wave energy is reflected at the transition zone.

4. Conclusion

A computational technique based on a combination of MD and FE methods has been implemented and tested on the propagation of a pressure wave induced by laser irradiation of an organic solid. Good agreement of both the total energy of the wave and the wave profile in MD and FE parts is observed in the simulation. The real strength of this combined approach is that a pressure wave can be transported over micron dimensions without losing the essential characteristics of the wave profile. Certainly improvements can be made. For example, nonlinear elasticity, anisotropy, and heat transfer can be included in the FE method. For our application, however, it is doubtful that any of these changes would improve the agreement between the pressure profiles shown in Fig. 4. An improvement could be achieved by decreasing the grid spacing in the FE region. This would lead to an increased memory requirement for the multiplication of matrices in the FE calculation as well as an increase in computer time. Ultimately each specific application determines

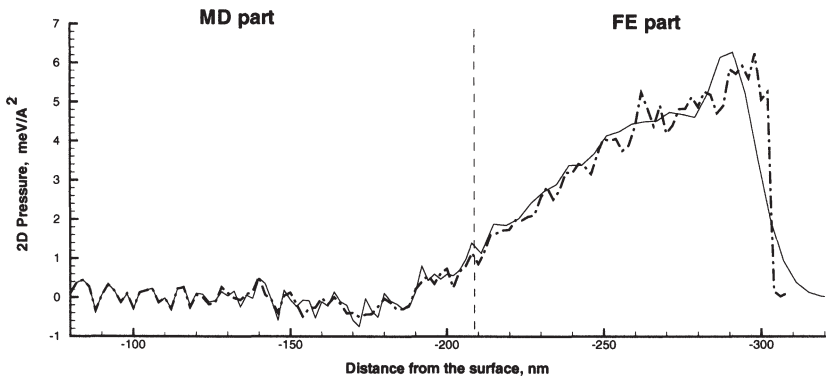

Fig. 4. The pressure wave profile in the MD–FE system and the reference pure MD system at 100 ps. The solid line is for the combined MD–FE system and the dash-dotted line is for the pure MD system.

its own tolerable accuracy and acceptable level of distortions caused by a more course space resolution in the FE method.

In summary, the combined MD–FE technique allows one to balance the level of details necessary to provide reasonable accuracy in some regions of the model with computational cost. In the field of laser ablation this approach can readily be applied to study back spallation, acoustic desorption, or laser ablation/damage of heterogeneous systems with spatially localized absorbers.

Acknowledgements

We gratefully acknowledge financial support from the National Science Foundation and the IBM Selected University Research Program. The computational support for this work was provided by Center of Academic Computing at Penn State University.

References

[1] M.P. Allen, D.J. Tildesley, Computer Simulation of Liquids (Clarendon Press, Oxford, 1987).
[2] R.S. Taylor, B.J. Garrison, Langmuir 11 (1995) 1220.
[3] B.J. Garrison, K.B.S. Prasad, D. Srivastava, Chem. Rev. 96 (1996) 1327.
[4] F.F. Abraham, Europhys. Lett. 38 (1997) 103.
[5] P.S. Lomdahl, R. Thompson, B.L. Holian, Phys. Rev. Lett. 76 (1996) 2318.
[6] J.H. Argyris, H.-P. Mlejnek, Dynamics of Structure (Elsevier, Amsterdam, 1991).
[7] T. Belytschko, T.J.R. Hughes, eds., Computational Methods for Transient Analysis (Elsevier, Amsterdam, 1983).
[8] L.V. Zhigilei, P.B.S. Kodali, B.J. Garrison, J. Phys. Chem. B 101 (1997) 2028; Chem. Phys. Lett. 276 (1997) 269; J. Phys. Chem. B 102 (1998) 2845.
[9] M. Moseler, J. Nordiek, H. Haberland, Phys. Rev. B 56 (1997) 15439.
[10] S. Kohlhoff, P. Gumbsh, H.F. Fischmeister, Phil. Mag. A 64 (1991) 851.
[11] L.V. Zhigilei, B.J. Garrison, in: Laser-Tissue Interaction IX, S.L. Jacques, ed., Proc. SPIE 3254 (1998) 135.
[12] I. Gilath, in: High-Pressure Shock Compression of Solids II, L. Davison, D.E. Grady, M. Shahinpoor, eds. (Springer, New York, 1996) p. 90.
[13] V.V. Golovlev, S.L. Allman, W.R. Garrett, N.I. Taranenko, C.H. Chen, Int. J. Mass Spec. Ion Process. 169/170 (1997) 69.
[14] S.L. Jacques, A.A. Oraevsky, R. Thompson, B.S. Gerstman, in: Laser-Tissue Interaction IX, S.L. Jacques, ed., Proc. SPIE 2134A (1994) 54.
[15] X. Wen, D.E. Hare, D.D. Dlott, Appl. Phys. Lett. 64 (1994) 184.
[16] M. Mullins, M.A. Dokainish, Phil. Mag. A 46 (1982) 771.
[17] E.B. Tadmor, M. Ortiz, R. Phillips, Phil. Mag. A 73 (1996) 1529.
[18] O.C. Zienkiewicz, R.L. Taylor, The Finite Element Method (McGraw-Hill, London, 1989).
[19] L.V. Zhigilei, B.J. Garrison, Appl. Surf. Sci. 127–129 (1998) 142.
[20] L.V. Zhigilei, B.J. Garrison, Appl. Phys. Lett. 71 (1997) 551; Rapid Commun. Mass Spectrom. 12 (1998) 1273.
[21] P.-O. Esbjørn, E.J. Jensen, J. Phys. Chem. Solids 37 (1976) 1081.
[22] J.M. McGlaun, P. Yarrington, in: High-Pressure Shock Compression of Solids, J.R. Asay, M. Shahinpoor, eds. (Springer, New York, 1993) p. 323.